Proceedings of the 8th International Symposium
on Experimental and Computational
Aerothermodynamics of Internal Flows
Lyon, July 2007
Paper reference : ISAIF8-00130

Analysis of Turbulent Free Convection in a Rectangular Rayleigh-Bénard Cell

M. Kaczorowski and C. Wagner

DLR – Institute of Aerodynamics and Flow Technology, Bunsenstr. 10, D-37073 Göttingen, Germany

The present study compares results of direct numerical simulations of thermal convection within a rectangular geometry with Rayleigh-Bénard convection in infinitely extended fluid layers and cylindrical geometries. It is shown that boundary layer thicknesses show similar tendencies in the rectangular geometry and the infinitely extended fluid layer simulated by Hartlep *et al.* [6], but the quasi two-dimensional geometry of the rectangular cell delays the transition to a 3-D flow. Energy spectra are evaluated at different locations of the flow field. The spectra recorded in the centre of the cell show the same exponential scaling within the equilibrium range as those obtained by Verzicco and Camussi [11] in a slender cylindrical container. However, it is observed that within the thermal boundary layer significantly more turbulent energy is held by the small scales which is reflected by a fuller spectrum and a smaller exponent. Analysis of the thermal dissipation rates indicates that there are three distinct regimes, with the small scale contributions growing rapidly for increasing Rayleigh number, whereas the large scale contributions remain almost constant.

Keywords: DNS, thermal dissipation rate, boundary layer, energy spectrum

Introduction

A well-studied, but yet not fully understood problem in fluid mechanics is the Rayleigh-Bénard convection, where fluid between horizontal walls is heated from below and cooled from above. The Rayleigh number

$$Ra = \alpha g H^3 \frac{\Delta T}{\kappa \nu} \qquad (1)$$

is a non-dimensional characteristic measure of the forces driving thermal convection determined by the height H of the fluid layer, the temperature difference between hot and cold wall ΔT, the gravitational acceleration g and the fluid properties α, κ and ν which are the thermal expansion coefficient, thermal diffusivity and kinematic viscosity respectively.

Typically, numerical experiments of the Rayleigh-Bénard problem assume periodic boundary conditions in horizontal direction or a cylindrical container. However, Daya and Ecke [2] studied the impact of the container shape on the turbulent properties, and interestingly found that temperature and velocity fluctuations strongly depend upon the geometry while global properties, such as heat transfer, remain unchanged within measurement accuracy.

In recent studies Verzicco and Camussi [10,11] have carried out direct numerical simulations of turbulent convection within cylindrical containers of low aspect ratio $\Gamma = D / H$, where D denotes the diameter of the container. They found that for a container of aspect ratio unity and Pr = 0.7 there is a transition from $\delta_\theta > \delta_u$ to $\delta_\theta < \delta_u$ around $Ra = 2 \times 10^7$, where δ_θ and δ_u denote the thermal and the kinetic boundary layer thickness respectively.

This phenomenon matches Grossmann and Lohse's theory [3]. However, they point out that according to theoretical analysis this transition should not occur until $Ra \approx 10^8$.

Shishkina and Wagner [9] have conducted direct numerical simulations of Rayleigh-Bénard convection in a wide cylindrical geometry. They analysed the contribution of thermal dissipation rates due to the turbulent background and the plumes, confirming Grossman and Lohse's theory by showing that the influence of the thermal turbulent background on the flow field increases with increasing Ra.

It is the aim of the present study to analyse turbulent thermal convection within a rectangular geometry. Thermal dissipation rates in a rectangular cell of aspect ratio unity and periodic boundary conditions in longitudinal direction are compared with the above mentioned results extracted from cylindrical geometries. In addition, the influence of the lateral wall is analysed comparing the results with simulations employing cyclic boundary conditions in two horizontal directions.

Nomenclature

E	energy
g	gravitational acceleration
h	length scale
H	height of the fluid layer / container
L	length of the container
Nu	Nusselt number
Pr	Prandtl number
Ra	Rayleigh number
$\Delta\hat{T}$	temperature difference [K]
u_i	velocity components
V	fluid volume / volume of the container
W	width of the container

Greek letters

α	thermal expansion coefficient
β	effective exponent
δ	boundary layer thickness
ε	dissipation rate
η	Kolmogorov length scale
θ	nondimensional temperature
κ	thermal diffusivity
ν	kinematic viscosity
Γ	aspect ratio of the container

Subscripts

t	top
b	bottom
u	velocity field
θ	temperature field

Computational Setup

The incompressible Navier-Stokes equations are solved in dimensionless form, where density variations are accounted for through the Boussinesq approximation.

$$\frac{\partial u_i}{\partial x_i} = 0$$

$$\frac{\partial u_i}{\partial t} = u_j \frac{\partial u_i}{\partial x_j} - \frac{\partial p}{\partial x_i} + \sqrt{\frac{\mathrm{Pr}}{\Gamma^3 Ra}} \frac{\partial^2 u_i}{\partial x_j^2} + \theta \delta_{1i} \quad (2)$$

$$\frac{\partial \theta}{\partial t} = u_i \frac{\partial \theta}{\partial x_i} + \sqrt{\frac{1}{\Gamma^3 Ra\,\mathrm{Pr}}} \frac{\partial^2 \theta}{\partial x_i^2}$$

The variables are non-dimensionalised with respect to the width W of the cell as well as buoyancy and the temperature difference between top and bottom walls.

$$x_i = \frac{\hat{x}_i}{W} \quad u_i = \frac{\hat{u}_i}{\sqrt{\alpha g H \Delta T}} \quad p = \frac{\hat{p}}{\rho \alpha g H \Delta T}$$
$$\theta = \frac{\hat{T} - \hat{T}_0}{\Delta \hat{T}} \quad t = \frac{\hat{t}\sqrt{\alpha g H \Delta T}}{W} \quad (3)$$

The solution is evolved in time by means of the Euler-Leapfrog scheme, and spatial derivatives are approximated by fourth order accurate central differences where the velocity components are stored on staggered grids [8]. In order to sufficiently resolve the boundary layers the grid points are clustered in the vicinity of the walls using a hyperbolic tangential. The grid spacing $h_{DNS} = (\Delta x\, \Delta y\, \Delta z)^{1/3}$ in the core region satisfies Grötzbach's [5] estimate for the Kolmogorov scales η_K.

$$h_{DNS} \le \eta_K = \frac{\pi}{\Gamma} \frac{\mathrm{Pr}}{\left((Nu-1)Ra\right)^{1/4}} \quad (4)$$

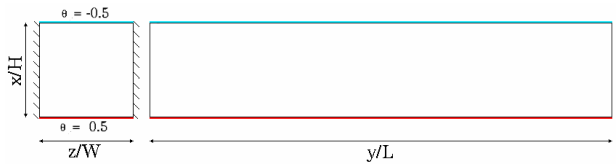

Fig. 1 Schematic of front and side view of the convection cell; $H = W = 1$ and $L = 5$

The horizontal walls are assumed to be isothermal with non-dimensional temperatures $\theta_b = +0.5$ and $\theta_t = -0.5$ at the top and bottom wall respectively. The adiabatic lateral walls are implemented by means of a zero temperature gradient perpendicular to the wall, i.e.

$\partial\theta / \partial z = 0$. No-slip conditions are used for the solid walls, so that velocities in *i*-direction $u_i \mid_{\text{wall}} = 0$, $i = 1,2,3$ and periodic boundary conditions are employed in longitudinal direction.

The computational domain is initialised with a quiescent velocity field and the conduction profile for the temperature field. Additionally, small disturbances are superimposed onto the temperature field at a single point and along a horizontal line in periodic direction. These disturbances are introduced in order to excite instabilities, and hence to trigger convection.

The solution is evolved in time until the flow field is in equilibrium, i.e. heat transfer between hot and cold walls and turbulence intensity have reached a quasi steady state. During the subsequent processing all characteristic flow parameters are averaged in time and space (periodic direction) to allow for a statistical analysis.

Results

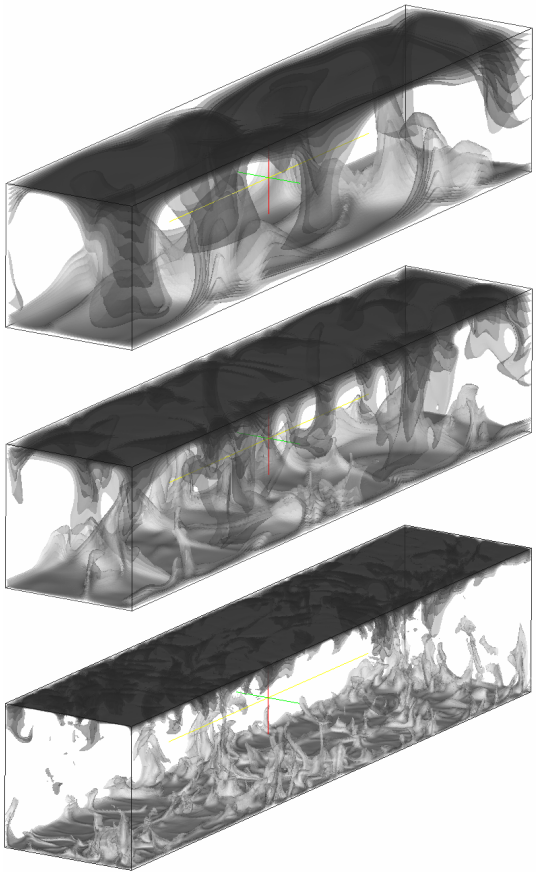

Fig. 2 Snapshots of the turbulent temperature fields showing the number and size of the thermal plumes for Rayleigh numbers $Ra = 4.4 \times 10^5$ (top), $Ra = 4.4 \times 10^6$ and $Ra = 7.5 \times 10^7$ (bottom); hot fluid is white and cold black.

Four direct numerical simulations of turbulent thermal convection within a rectangular cell have been carried out for Rayleigh numbers up to 7.5×10^7. Figure 2 shows snapshots of the turbulent temperature fields for three Rayleigh numbers, indicating that the number of thermal plumes is increasing and their size decreasing with Rayleigh number.

Energy Spectra

Figure 3 illustrates thermal and kinetic energy spectra taken from probes within the conductive sublayer and the core of the domain ($x/H = 0.5$) midway between the lateral walls ($z/W = 0.5$), averaged in time and periodic direction. It can be seen that the temperature spectra in the center of the cell match the Bolgiano exponent [1] of 7/5 very well, but lack the inertial subrange which is supposed to follow the buoyancy subrange. According to the Bolgiano dynamics the velocity spectra should show a 11/5 decrease within the buoyancy subrange, but only the Kolmogorov law is observed. This is in agreement with results by Verzicco and Camussi [11] who argued that this might be the case, when most of the thermal energy is injected into the large scales through the wind.

However, one also has to take into account that the Bolgiano dynamics assume a stably stratified fluid layer. In the case of Rayleigh-Bénard convection energy is injected into the fluid by means of thermal plumes which are the driving force for convection as shown by Xi *et al.* [12]. It is therefore reasonable that the velocity spectra follow the Kolmogorov law, since there is no energy extracted from the velocity field and stored as potential energy as suggested by Bolgiano's theory.

It can be assumed that all relevant turbulent scales are resolved by the grid, since both the inertial subrange and the dissipation range can be clearly identified from the kinetic energy spectra and the Batchelor scales of temperature are larger than the Kolmogorov scales; $\eta_B / \eta_K = \mathrm{Pr}^{-3/4}$.

In the vicinity of the horizontal walls a different scaling is observed, since the wall tends to damp the wall normal velocity component, which is also reflected by the temperature spectra which have significantly smaller exponents within the equilibrium range: e.g. 0.7 for $Ra = 4.4 \times 10^6$ and 0.5 for $Ra = 7.5 \times 10^7$. Following the above reasoning and taking into account that the entire heat transfer takes place within the thermal boundary layer, it can be concluded that more energy is injected into the small scale structures, since large scales structures are suppressed in the increasingly thinner boundary layers. This is also substantiated by a fuller temperature spectrum towards the high wave number cut-off. The analysis of spectra at different distances from the horizontal walls shows that the exponent of the buoyancy range is asymptotically approaching the Bolgiano exponent, whereas the level of energy held by the respective scales is slowly decreasing.

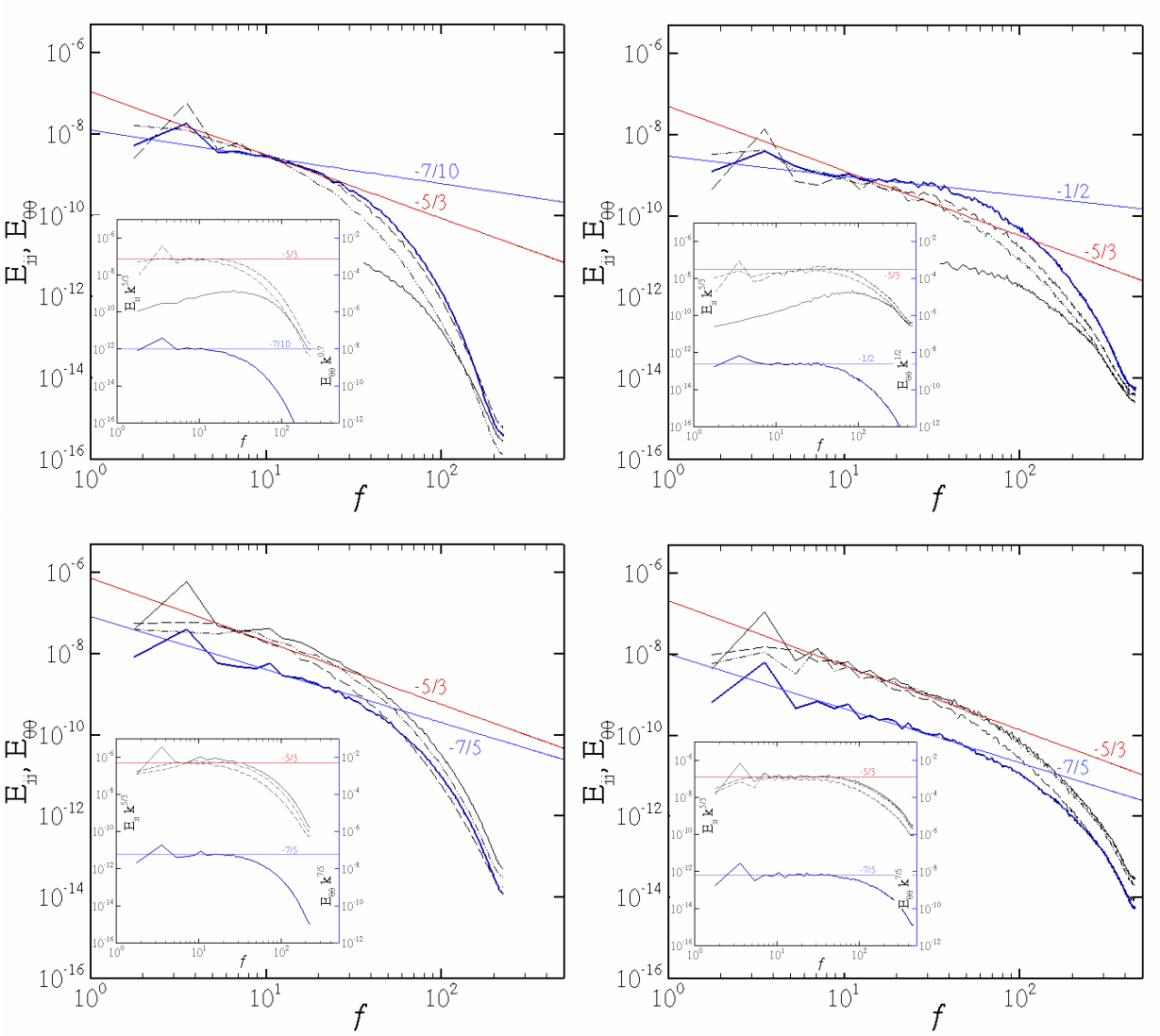

Fig. 3 Energy spectra for $Ra = 4.4 \times 10^6$ (left) and $Ra = 7.5 \times 10^7$ (right) extracted from the conductive sublayer (top) and the centre of the cell, $x/H = 0.5$, (bottom) at $z/W = 0.5$. E_{uu} (—), E_{vv} (- - -), E_{ww} (- • • -) and $E_{\theta\theta}$ (—). The insets show the respective compensated spectra.

Scaling Law

Figure 4 shows the Nusselt number Nu as a function of Rayleigh number from $Ra = 4.4 \times 10^4$ up to $Ra = 7.5 \times 10^7$. When comparing the regimes with data gathered by Krishnamurti [7] and numerical simulations of convection within an infinitely extended fluid layer (Hartlep *et al.* [6]), it follows that the transition to turbulence occurs at $Ra \approx 10^5$ rather than $\mathrm{Ra} \approx 10^4$.

Given a scaling law of the form $Nu \sim Ra^{\beta}$ an effective exponent $\beta \approx 0.284$ is obtained which is in good agreement with the theoretical prediction [4] $\beta \approx 2/7$ (≈ 0.286) for $Ra \leq 10^{11}$ and Pr = 0.7. Finally, it can be concluded that even though the onset of convection does not seem to be significantly delayed the quasi two-dimensional shape of the container seems to stabilize the three-dimensional modes, and hence delays the transition to a three-dimensional flow field.

Boundary Layer Thicknesses

The viscous and thermal boundary layer thicknesses have been measured at $z/W = 0.5$ for Rayleigh numbers up to $Ra = 7.5 \times 10^7$. It follows from figure 5 that the boundary layers are decreasing at different rates, suggesting that there might be a cross-over of the boundary layer thicknesses for $Ra < 8.8 \times 10^4$. However, for lower Ra the flow field is steady and laminar, and hence the definition of the edge of the boundary layer through the maximum-rms-value criterion does not hold anymore.

However, it can be observed that the results by Hartlep *et al.* [6] show similar tendencies and, despite that fact that the transition to 3-D flow occurs at significantly different Ra, the boundary layer thicknesses are almost the same.

A comparison with Verzicco and Camussi's data [11] reveals a similar behaviour of the boundary layers.

However, it has to be pointed out that the cross-over from one regime ($\delta_\theta > \delta_u$) to the other ($\delta_\theta < \delta_u$) is significantly delayed in their low aspect ratio cylindrical cell, i.e. $Ra \approx 10^7$ rather than $Ra \approx 10^4$ in the rectangular cell or Ra $\approx 10^5$ in the infinitely extended fluid layer by Hartlep *et al.* [6].

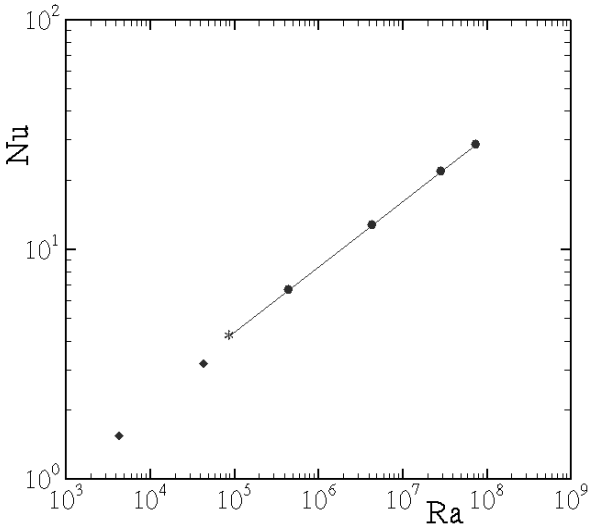

Fig. 4 Nusselt number as a function of Rayleigh number for $4.4 \times 10^3 < Ra < 7.5 \times 10^7$; laminar (♦), 3-D periodic time dependent (*) and turbulent flow (●); Nu ~ $Ra^{0.284}$ (---).

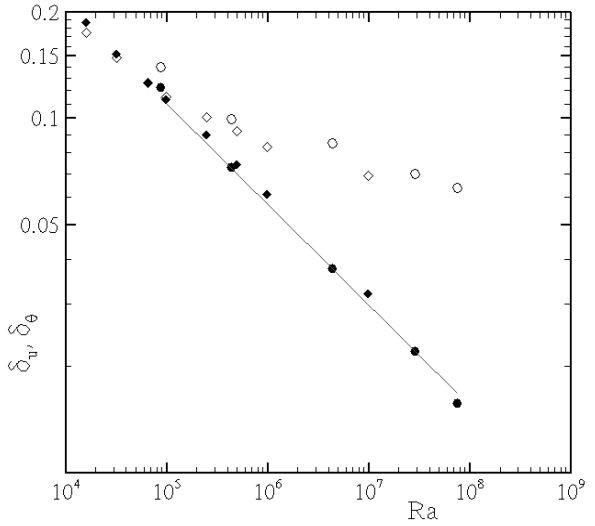

Fig. 5 Viscous (○) and thermal (●) boundary layer thickness as a function of Rayleigh number for $8.8 \times 10^4 \le Ra \le 7.5 \times 10^7$ at $z/W = 0.5$; $\delta_\theta \sim Ra^{-0.284}$ (---). Diamonds indicate data by Hartlep *et al.* [6] for an infinitely extended thin fluid layer.

Shape of the Thermal Boundary Layer

The shape of the thermal boundary layers is analysed for the simulations with Rayleigh numbers $Ra = 4.4 \times 10^5$, $Ra = 4.4 \times 10^6$ and $Ra = 7.5 \times 10^7$. Figure 6 shows that in the vicinity of the horizontal walls an exponent of $\alpha = 1$ matches all three temperature profiles very well. This is reasonable, since conduction rather than convection is supposed to dominate the flow field in this region.

It can also be seen from the below plot that about 6 and 4 and 3 grid points are within the conductive sublayer for $Ra = 4.4 \times 10^5$, $Ra = 4.4 \times 10^6$ and $Ra = 7.5 \times 10^7$ respectively. Due to Grötzbach [5] a minimum of 3 points is required in this region in order to sufficiently resolve the thermal boundary layer.

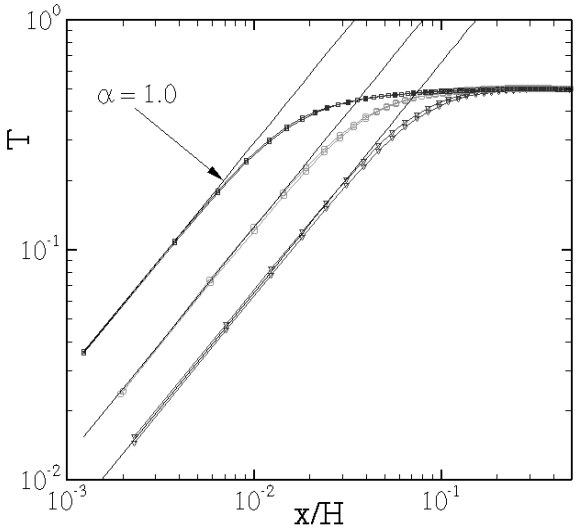

Fig. 6 Shape of the spatially and temporally averaged conductive sublayer at $z/W = 0.5$. $Ra = 4.4 \times 10^5$ (▼), $Ra = 4.4 \times 10^6$ (○) and $Ra = 7.5 \times 10^7$ (□); $T = 0.5 - |\theta| \sim (x/H)^\alpha$ (—).

Thermal Dissipation Rates

Statistical analysis of the thermal dissipation rates is carried out following the approach by Shishkina and Wagner [9] who introduced two functions

$$\tau(\xi) = \left\langle \vartheta(\xi\varepsilon_{\theta,\max} - \varepsilon_\theta) \right\rangle_V \tag{5}$$

and

$$\sigma(\xi) = \frac{\left\langle \varepsilon_\theta \, \vartheta(\xi\varepsilon_{\theta,\max} - \varepsilon_\theta) \right\rangle_V}{\left\langle \varepsilon_\theta \right\rangle_V} \tag{6}$$

where

$$\vartheta(x) = \begin{cases} 1; & x \ge 0 \\ 0; & \text{otherwise} \end{cases} \tag{7}$$

which determine the percentage of the fuid volume with dissipation rates less than ξ times the volume averaged thermal dissipation rate $\varepsilon_{\theta,\max}\big|_V$ and its contribution to the volume averaged thermal dissipation rate respectively.

Thus, the role of plumes and thermal background can be determined, when taking into account that large thermal dissipation rates can be associated with a thermal plume and small dissipation rates are characteristic for

the turbulent background.

Figure 7 illustrates that with increasing Rayleigh number the percentage of the fluid volume $\tau(\xi)$ for a given ξ increases as well as its contribution to the volume averaged thermal dissipation rate. Hence, it follows that smaller scales begin to dominate the thermal dissipation.

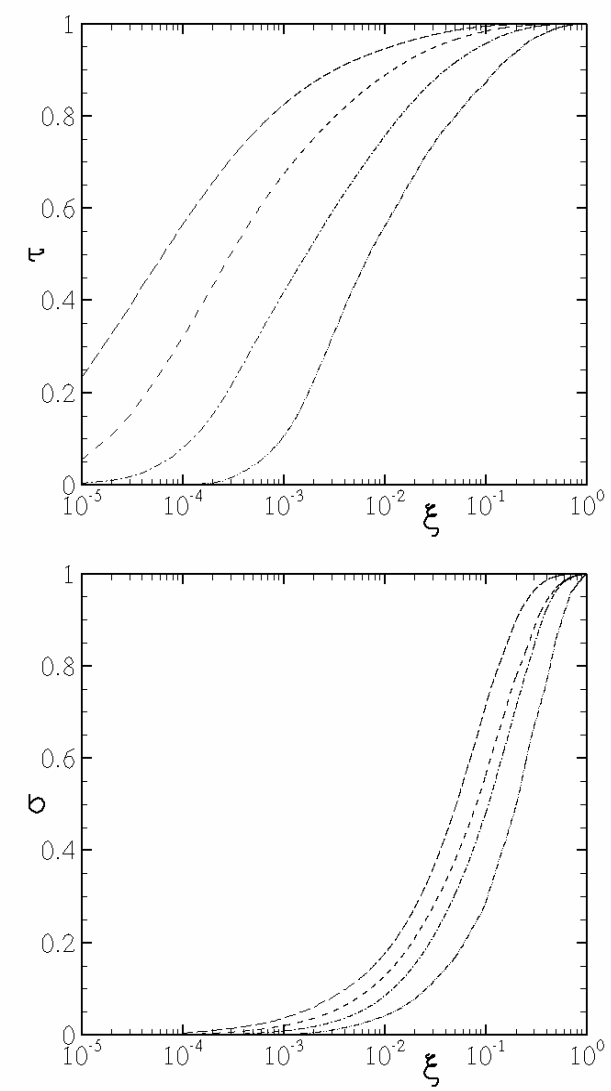

Fig. 7 Fraction of the fluid volume containing thermal dissipation rates $\varepsilon_\theta \le \xi\ \varepsilon_{\theta,\max}\big|_V$ (top) and their contribution to the volume averaged thermal dissipation rate (bottom); $Ra = 8.8 \times 10^4$ (– · · –), $Ra = 4.4 \times 10^5$ (– · –), $Ra = 4.4 \times 10^6$ (- - -) and $Ra = 2.3 \times 10^7$ (– – –).

Investigation of the dissipation rate distribution as a function of ξ displays their respective contribution to the mean dissipation rate and reveals that there is a predominant range of dissipation rates. It can be seen from figure 8 that the location of the maximum of this function is decreasing with Rayleigh number, indicating that small dissipation rates, and hence the turbulent background becomes increasingly important at higher Rayleigh numbers.

Once the flow field has become turbulent three distinct regimes can be identified from the scatter plot of the dissipation rate distribution. The regime $\xi \to 1$ that is associated with thermal plumes and boundary layers appears to maintain its shape, but rises slightly as Rayleigh number increases. The lower tail ($\xi \to 0$) of the function is, however, strongly dependent on the Rayleigh number as the contribution of these scales increases significantly as Ra increases. For $Ra = 8.8\times 10^4$, where the flow field is laminar, but three dimensional, these tails form a bell shape-like distribution, whereas the tails are joined by a linear regime when turbulence sets in.

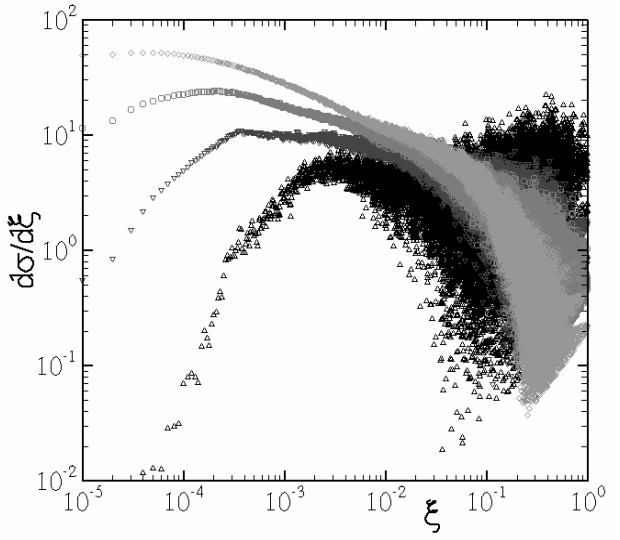

Fig. 8 Contribution of the thermal dissipation rates with $\varepsilon_\theta = \xi\ \varepsilon_{\theta,\max}\big|_V$ to the volume averaged thermal dissipation rate. $Ra = 8.8\times 10^4$ (Δ), $Ra = 4.4 \times 10^5$ (▼), $Ra = 4.4 \times 10^6$ (○) and $Ra = 2.3 \times 10^7$ (◊).

Conclusions

Direct numerical simulations of Rayleigh-Bénard convection have been conducted in a rectangular cell with periodic boundaries in longitudinal direction. It is found that compared to experimental and numerical investigations in wide geometries the transition to a 3-D flow is delayed in the periodic rectangular cell. However, the tendencies and thicknesses of the boundary layers are very similar to those observed boundary by Hartlep *et al* [6].

The kinetic energy spectra recorded in the centre of the cell match the Kolmogorov law very well, whereas the thermal spectra achieve an exponent of 7/5 within the equilibrium range. Towards the isothermal walls the wall normal velocity component is damped, and hence the exponent of the equilibrium range is decreasing rapidly in the vicinity of the wall. It is also observed that in this

region significantly more energy is held within the high wave number range of the temperature spectrum as Rayleigh number is increasing. This is thought to be a result of the decreasing boundary layer thickness, which can only contain large scale structures of the order of its own thickness. Hence, more thermal energy has to be injected into the small scales, i.e. the background turbulence.

From the analysis of the thermal dissipation rates it is found that there are three distinct regimes of large, small and intermediate scales that are associated with the near wall region, plumes and background turbulence. From the distribution of the thermal dissipation rates it follows that the small scales, and hence the thermal background turbulence is increasing, whereas the large dissipation rates hardly change with Rayleigh number. However, further analysis is required to identify the respective parts that contribute to each regime.

Acknowledgement

The authors would like to thank the Helmholtz Association of German Research Centers (HGF) for funding the project "*Virtual Institute – Thermal Convection*".

References

[1] Bolgiano, R.: Turbulent Spectra in a Stably Stratified Atmosphere, J. Geophys. Res., vol. 64 (12), pp. 2226 －2229, (1959).

[2] Daya, Z. A. and Ecke, R. E.: Does Turbulent Convection Feel the Shape of the Container?, Phys. Rev. Lett., vol. 87, pp. 184501－184504, (2001).

[3] Grossmann, S. and Lohse, D.: Scaling in thermal convection: a unifying theory, J. Fluid Mech., vol. 407, pp.27－87, (2000).

[4] Grossmann, S. and Lohse, D.: Fluctuations in turbulent Rayleigh-Bénard convection: The role of plumes, Phys. Fluids, vol. 16(12), pp. 4462－4472, (2004).

[5] Grötzbach, G.: Spatial Resolution Requirements for Direct Numerical Simulation of Rayleigh-Bénard Convection, J. Comp. Phys., vol. 49, pp.241－264, (1983).

[6] Hartlep, T., Tilgner, A. and Busse, F. H.: Transition to turbulent convection in a fluid layer heated from below at moderate aspect ratio, J. Fluid Mech., vol. 554, pp.309－322, (2005).

[7] Krishnamurti, R.: Some further studies on the transition to turbulent convection, J. Fluid Mech., vol. 60, pp. 285－303, (1973).

[8] Shishkina, O. and Wagner, C.: A fourth order finite volume scheme for turbulent flow simulations in cylindrical domains, Computers and Fluids, vol. 36 (2), pp. 484－497, (2007).

[9] Shishkina, O. and Wagner, C.: Analysis of thermal dissipation in turbulent Rayleigh-Bénard convection, J. Fluid Mech., vol. 546, pp. 51－60, (2006).

[10] Verzicco, R. and Camussi, R.: Prandtl number effects in convective turbulence, J. Fluid Mech., vol. 383, pp. 55－73, (1999).

[11] Verzicco, R. and Camussi, R.: Numerical experiments on strongly turbulent thermal convection in a slender cylindrical cell, J. Fluid Mech., vol. 477, pp. 19－49, (2003).

[12] Xi, H.-D., Lam, S. and Xia, K.-Q..: From laminar plumes to organized flows: the onset of large-scale circulation in turbulent thermal convection, J. Fluid Mech., vol. 503, pp. 47－56, (2004).